frontiers | Frontiers in Molecular Neuroscience

TYPE Original Research
PUBLISHED 03 September 2025
DOI 10.3389/fnmol.2025.1604262

OPEN ACCESS

EDITED BY
Richard Miller,
Northwestern University, United States

REVIEWED BY
Austen Sitko,
Harvard Medical School, United States
Marta Maria Nowacka-Chmielewska,
Jerzy Kukuczka Academy of Physical Education in Katowice, Poland

*CORRESPONDENCE
M. Dziembowska
✉ m.dziembowska@uw.edu.pl

RECEIVED 01 April 2025
ACCEPTED 01 August 2025
PUBLISHED 03 September 2025

CITATION
Chojnacka M, Skupien-Jaroszek A and Dziembowska M (2025) Delayed structural maturation of inner hair cell ribbon synapses in a mouse model of fragile X syndrome. *Front. Mol. Neurosci.* 18:1604262. doi: 10.3389/fnmol.2025.1604262

Delayed structural maturation of inner hair cell ribbon synapses in a mouse model of fragile X syndrome

M. Chojnacka, A. Skupien-Jaroszek and M. Dziembowska*

Faculty of Biology, Institute of Experimental Zoology, University of Warsaw, Warsaw, Poland

Clinical features of the fragile X syndrome (FXS) phenotype include intellectual disability, repetitive behaviors, social communication deficits, and, commonly, auditory hypersensitivity to acoustic stimuli. Electrophysiological studies have shown that FXS patients and Fmr1KO mice exhibit improper processing of auditory information in the cortical areas of the brain and the spiral ganglion of the cochlea. Synapses formed by spiral ganglion neurons on sensory hair cells (HC) are the first connection on the path that conveys the auditory information from the sensory cells to the brain. We confirmed the presence of fragile X mental retardation protein (FMRP) in the inner hair cells of the cochlea. Next, we analyzed the morphology of IHC ribbon synapses in early stages of postnatal development (P5, P14) and detected their delayed structural maturation in Fmr1 KO mice. Interestingly, the ultrastructure of inner hair cell ribbon synapses, studied by electron microscopy in adult mice (P48), has shown no specific dysmorphologies. Delayed structural maturation of presynaptic ribbons of auditory hair cells in Fmr1 KO mice may contribute to abnormal development of circuits induced by auditory experience.

KEYWORDS

fragile X syndrome, FMRP, inner hair cell, ribbon synapses, electron microscopy, organ of Corti

Introduction

Fragile X syndrome (FXS) is a genetic disorder caused by transcriptional silencing of the FMR1 gene on chromosome X (Hagerman et al., 2017; Hagerman et al., 2005). The FMR1 gene contains nearly 50 CGG trinucleotide repeats in the 5′ untranslated region, but in FXS the repeats expand to over 200, this leads to hypermethylation in the expanded CGG repeats and no expression of FMRP protein (Crawford et al., 2001). FXS is the most common monogenic cause of inherited intellectual disability and autism spectrum disorder (Sinclair et al., 2017). FXS patients are often characterized by poor language development and prominent sensory abnormalities (Hagerman et al., 2017; Rais et al., 2018). In both FXS patients and animal models, studies show auditory hypersensitivity, impaired habituation to repeated sounds, reduced auditory attention, and difficulties in complex listening, phenotypes that may also be associated with problems in social interactions and language development (Rotschafer and Razak, 2013; Rotschafer and Razak, 2014; Rais et al., 2018; Razak et al., 2021).

The critical element of the mammalian auditory system located in the organ of Corti are hair cells, the auditory receptors that form synapses with spiral ganglion neurons and transform mechanical vibrations into electrical signals (Wichmann and Moser, 2015). Two types of sensory hair cells are located in the organ of Corti, the inner hair cells IHC and outer hair cells OHC connected to SGNs by glutamatergic ribbon synapses, which are essential for faithful synaptic transmission (Glowatzki and Fuchs, 2002). The IHCs possess highly

specialized presynaptic active zones (AZs) called synaptic ribbons with the characteristic RIBEYE protein stem and synaptic vesicles docked into it. Ribbon synapses of cochlear inner hair cells (IHCs) undergo molecular assembly and extensive functional and structural maturation prior to the onset of hearing. This maturation is critical, as the molecular architecture of ribbon synapses is closely linked to their physiological properties. Previous studies have demonstrated that ribbon size can influence the frequency of miniature excitatory postsynaptic currents (mEPSCs), supporting the role of ribbons in coordinating multivesicular release (Mehta et al., 2013; Wichmann and Moser, 2015). More recent findings indicate that structural and functional abnormalities in ribbon synapses contribute to sensorineural hearing loss (Liberman and Kujawa, 2017).

The majority of studies investigating synaptic structure and function in fragile X syndrome (FXS) have focused on central nervous system (CNS) circuits, particularly within cortical and hippocampal regions. In both *Fmr1* knockout (Fmr1KO) mice, an established animal model of FXS, and in human patients, dendritic spines exhibit characteristically altered morphology and are long, thin and philopodial in shape (Comery et al., 1997). By contrast, significantly less is known regarding potential synaptic and structural abnormalities in the peripheral nervous system (PNS) of individuals with FXS. Notably, the PNS includes critical pathways such as the optic nerve and the afferent connections between spiral ganglion neurons and inner hair cells, which may also be susceptible to FMRP-related dysfunction. This led us to investigate the abundance of synaptic connections in hair cells of Fmr1KO mice compared to those of wild-type mice.

In this study, we performed morphological analysis of IHCs in the wt and Fmr1KO mice cochleae using complementary research methods that included confocal and electron microscopy imaging. This allowed us to study the morphology of the IHC in the organ of Corti at three developmental stages: P5, P14, and P48. With the EM we imaged the fine structure of IHCs ribbon synapses in adult mice P48 and found no visible morphological differences in IHC morphology, distribution of mitochondria, the number of presynaptic active zones and postsynaptic neurites of SGNs when we compared Fmr1KO and WT mice. The ultrastructure of reconstructed ribbons did not show any particular dysmorphologies or differences in the number of synaptic vesicles. However, using immunofluorescent staining of presynaptic ribbons performed on three developmental stages spanning prehearing (P5), hearing onset (P14), and adulthood, we identified a delayed formation of ribbon synapses in the cochlear inner hair cells.

Materials and methods

Animals

We used male *Fmr1* knockout (*Fmr1* KO) mice on FVB background (FVB.129-Fmr1^{tm1Rbd}/J, RRID: IMSR_JAX:008909) and their wild-type (WT) littermates (P5, P14 and P48). The mice were genotyped accordingly to the Jackson Laboratory protocol. Mice were bred in the Animal House of the Faculty of Biology, University of Warsaw. The animals were kept in the laboratory animal facility under a 12-h light/dark cycle with food and water available ad libitum. The animals were treated in accordance with the EU Directive 2010/63/EU for animal experiments and Polish regulations. The mice were anesthetized with inhaled isoflurane (5% in the inhaled air) and euthanized by cervical dislocation.

Immunofluorescence staining of hair cells of organ of Corti

To obtain inner ears, animals were sacrificed according to approved humane protocol and the inner ears were dissected from the skull. Round and oval windows were opened, and bone over the apical turn removed to allow rapid fixation of 4% paraformaldehyde with 4% saccharose in PBS through the cochlear for 5 min. Next, cochleas were transferred into PBS, to obtain their apical turn. Bone over the middle-ear-facing portion of the cochlear spiral and the tectorial membrane were removed by fine forceps. Following tissue were fixated in 4% paraformaldehyde with 4% saccharose for 40 min. For blocking and permeabilization, cochleas were incubated in PBS with 0.5% Triton X-100 and 5% BSA for 1 h, with gentle shaking. Next, tissue was incubated with primary antibodies at 4 °C for overnight, and secondary antibodies Alexa Fluor (1:1,000; Invitrogen) at room temperature for 2 h. The following antibodies and fluorescent dyes were used: mouse IgG1 Anti-CtBP2 Clone 16/CtBP2 (1:500; BD Transduction Laboratories), mouse IgG2a anti-GluA2 (1:200; Millipore); rabbit anti-MyosinVI (KA-15) (1:1,000, Sigma); mouse IgG2a anti-Bassoon (1:500, Santa Cruz); rabbit anti-FMRP (D14F4) (1:100, Cell Signaling); Phalloidin 405 nm (1:1,000, Abcam), rabbit anti-Tom20 (FL-145) (1:250, Santa Cruz). After immunostaining, cochleas were mounted on microscope slides in ProLong Gold antifade reagent (Invitrogen), and coverslipped.

Confocal microscopy

Z-stacks from selected cochlear regions from each ear were obtained on confocal microscope (Zeiss Axio Imager Z2 LSM 700) with oil-immersion objective 63× and 1× digital zoom. Images were obtained in a 2,048 × 2,048 frame (pixel size = 0.05 µm in x and y). Care was taken to minimize pixel saturation in each image stack. Each stack contained the entire synaptic pole of eight to 11 inner hair cells as viewed from the surface of the organ of Corti. The same microscope settings were used for all sections and all repetitions.

Image analysis

The images were analyzed in the 3D Object Counter[1] application running in the ImageJ/Fiji. Intensity threshold settings were adjusted to identify the vast majority of synaptic densities, while excluding non-synaptic staining. The histogram depicting the frequency of ribbons as a function of the volume of the presynaptic, anti-CtBP2 stained puncta was performed using GraphPad Prism version 7.00 for Windows, GraphPad Software, La Jolla California United States, www.graphpad.com.

1 https://imagej.net/3D_Objects_Counter

Electron microscopy

To maintain proper structure of hair cells in samples collected from adult mice, we removed the membrane from the round window and the stapes footplate of the oval window, and opened a small hole in the bone at the apex of the cochlea. Next, solution for fixation were gently perfused by syringe and perfusion-fixed on ice over-night.

Transmission electron microscopy

The whole cochlea was cut out together with the bone capsule and transferred 2.5% glutaraldehyde (Electron Microscopy Sciences), 2% formaldehyde (fresh from paraformaldehyde EMS) in PBS at 4 °C overnight. After washing with PBS, the tissue was incubated in 1% osmium tetroxide and dehydrated in graded aqueous ethanol solutions from 25 to 96% (each for 10 min) followed by 100% ethanol (two lesions each for 10 min). Infiltrated with a mixture of 25% and epoxy resin 30 min on ice, 50% epoxy resin for 2 h, 75 and 100% for 24 h at room temperature Then, the samples in 100% epoxy resin were transferred to a flat embedding mold and placed in an oven at 60 °C for 48 h. Samples were cut on an ultramicrotome (Leica) by diamond Diatome knife (Ted Pella) into 100 µm thick slices. The ribbon was transferred to tungsten coated copper meshes and incubated with 1% uranyl acetate followed by lead aspartate. Electron micrographs were obtained on a transmission electron microscope JEM 1400 (JEOL).

Serial block face scanning electron microscopy

Tissue preparation using this protocol allowed for partial reconstruction of hair cell ultrastructure (Bullen et al., 2015). After fixation (cold 2% paraformaldehyde, 2.5% glutaraldehyde solution in PBS) and decalcification cochleas were transferred to 0.1% tannic acid (EMS, United States) in PBS and incubated in this solution overnight at 4 °C. Samples were processed for serial block face scanning electron microscopy (SBF-SEM) following the method of Deerinck et al. (2010). The samples were trimmed and mounted into pins. Smooth surface of sample to SBF-SEM was obtained by using ultramicrotome (Leica) and diamond knife (Ted Pella). Next, the sample were painted with silver paint (Ted Pella) for enhance conductivity. Samples were imaged by SBF-SEM Sigma VP 3View at the Nencki Institute of Experimental Biology through the technical platform (Laboratory of Imaging Tissue Structure and Function). Scanning parameters: variable pressure 25 Pa, EHT 3 kV, aperture 30um, dwell time 2–5 µs and 7–9 µs. Blocks were cut at 50 nm and 150 nm, and the exposed block face imaged with a pixel size of 3.7–4.2 nm and 10–11 nm for synapse and inner hair cells images, respectively.

The analysis of hair cells ultrastructure

3D models for whole cell, cellular organelles such as mitochondria and ribbon synapses in the hair cells of WT and Fmr1 KO mice were prepared using Reconstruct software (Fiala, 2005) http://synapses.clm.utexas.edu/tools/reconstruct/reconstruct.stm.

Statistics

All the statistical details including statistical tests used and number of biological replicates are described in the Figure Legends. The analyses were performed using Prism 10.4.0 software (GraphPad, San Diego, CA, United States).

Results

Expression of FMRP in the hair cells of the organ of Corti

We examined the expression of FMRP in the hair cells of mice. Staining was performed on tissue isolated from the cochlea of P5 and adult (P80) WT and Fmr1 KO mice ($n = 2$ per genotype for P5, $n = 3$ per genotype for adult mice). We used an anti-CtBP2 antibody as a marker for nuclei and synaptic ribbons in hair cells. Staining with an anti-FMRP antibody confirmed the presence of FMRP in the hair cells (inner and outer hair cells) of both young and adult WT mice (Figure 1).

Evaluation of the morphology of hair cells in Fmr1 KO and WT mice using confocal microscopy

The structural details of hair cells in the cochlea of Fmr1 KO mice have not been explored; therefore, we began our analysis by examining the structure of inner hair cells (IHCs) using confocal microscopy. We conducted immunofluorescence staining using specific antibodies that mark IHC and their pre- and postsynaptic compartments. The anti-CtBP2 antibody was utilized to stain both the synaptic ribbons and nuclei in the IHCs, while anti-Bassoon was used for the localization of the presynaptic active zone protein Bassoon, and anti-GluA2 for the postsynapse. Additionally, phalloidin was used to visualize the stereocilia, and myosin VI was used to stain the cell body. To observe mitochondria within the hair cells, we used the anti-Tom20 antibody (Figure 2).

The confocal microscopy images revealed the typical morphology of the IHCs in the cochleae of Fmr1KO mice. The stereocilia were situated on the apical part of the cell body, anchored to the cuticular plate (Figures 2A,B), with the nuclei located in the apical half of the cell. Mitochondria were distributed throughout the cell body (Figures 2F–H). The basal part of the IHCs housed multiple synaptic ribbons. Our findings show that the synaptic ribbons in IHCs from Fmr1KO mice are positioned opposite the AMPA glutamate receptors (indicated by GluA2 staining) on the postsynaptic side, within the afferent nerve fibers (Figures 2A,B, 3A–F).

Bassoon plays a crucial role in anchoring ribbons close to the presynaptic membrane. To study whether its level is unchanged in Fmr1KO IHC, we carried out immunostaining using anti-Bassoon and anti-CtBP2 antibodies. We observed that numerous Bassoon immunosignals overlapped with the ribbons in the IHCs of both WT and Fmr1KO mice. Additionally, there were distinct Bassoon signals that did not overlap, which likely originated from efferent nerve terminals (Figures 2D,E).

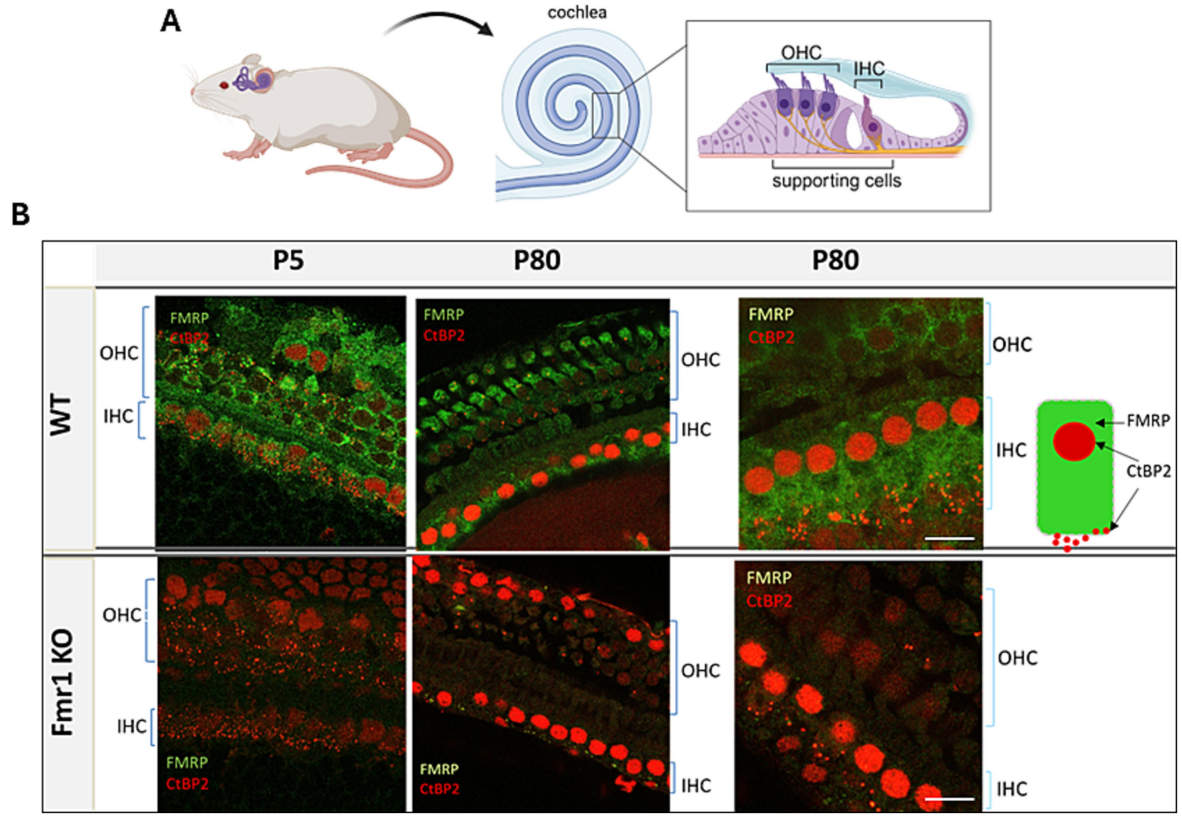

FIGURE 1
(A) Diagram showing the location of inner hair cells (IHC) and outer hair cells (OHC) in the organ of Corti in a mouse. **(B)** Representative images of the organ of Corti's from P5 and P80 mice WT—upper panel, Fmr1KO—lower panel. Inner hair cells (63× objective) from the middle turn (P5) and the apical turn (P80) of cochlea. Immunofluorescence staining using anti-CtBP2 (red) and anti-FMRP antibody (green), 63× objective. Scale bar 10 μm. Partially created with BioRender.

Quantitative analysis of ribbon synapses in hair cells of Corti's organ in Fmr1 KO and WT mice shows their delayed structural maturation

The structural maturation of ribbon synapses in inner hair cells (IHCs) is a complex process that is tightly regulated during early postnatal development. To investigate how ribbon synapses develop in *Fmr1* knockout (KO) IHCs compared to wild-type (WT) mice, we conducted confocal microscopy analyses to assess their volume across three developmental stages, from postnatal day 5 (P5) through P14 and adulthood P48 (Figure 3). These stages encompass both pre- and post-hearing onset periods.

To image the presynaptic ribbons we performed immunostaining using an anti-CtBP2 antibody on tissue isolated from the apical turns of the cochlea at P5, P14, and P48 mice (Figure 3). This approach enabled us to quantify the number of ribbon synapses per IHC and assess the distribution of their average size.

We observed that the number of CtBP2/RIBEYE puncta in IHCs significantly decreased from P5 to P14 (following the onset of hearing) and then stabilized. Although the number of synapses per IHC was comparable between wild-type and *Fmr1* KO mice (Figures 4A–C), the average volume of fluorescently labeled presynaptic ribbons was notably smaller in P14*Fmr1* KO mice across three litters (Figures 4D–F).

Histograms showing the distribution of average synapse sizes (categorized into arbitrarily defined size classes) revealed a higher prevalence of smaller ribbon synapses in the P14 Fmr1KO (0.04–0.18 μm^3), compared to a predominance of larger ribbons in wild-type littermates (0.2–0.6 μm^3) (Figures 4E, G–I). Although this difference in ribbon volume was less pronounced in adult mice, smaller synapses remained more prevalent in *Fmr1* KO mice at P48 (0.06–0.14 μm^3) relative to wild-type controls (0.16–0.44 μm^3) (Figure 4F).

Histograms representing the distribution of average synapse volume at P5 indicated that ribbons were comparable between wild-type and Fmr1KO animals at the early developmental stage before hearing onset (Figure 4D).

Inner hair cells ultrastructure in Fmr1 KO and WT mice using transmission electron microscopy and the serial block face scanning electron microscopy

The ultrastructure of hair cells in *Fmr1* KO mice has not been studied before, and the observed delay in the structural development of IHC ribbon synapses may influence their mature appearance. Therefore, to investigate the fine morphology of these cells, we employed two complementary methods based on electron microscopy: transmission electron microscopy (TEM) and serial

10.3389/fnmol.2025.1604262

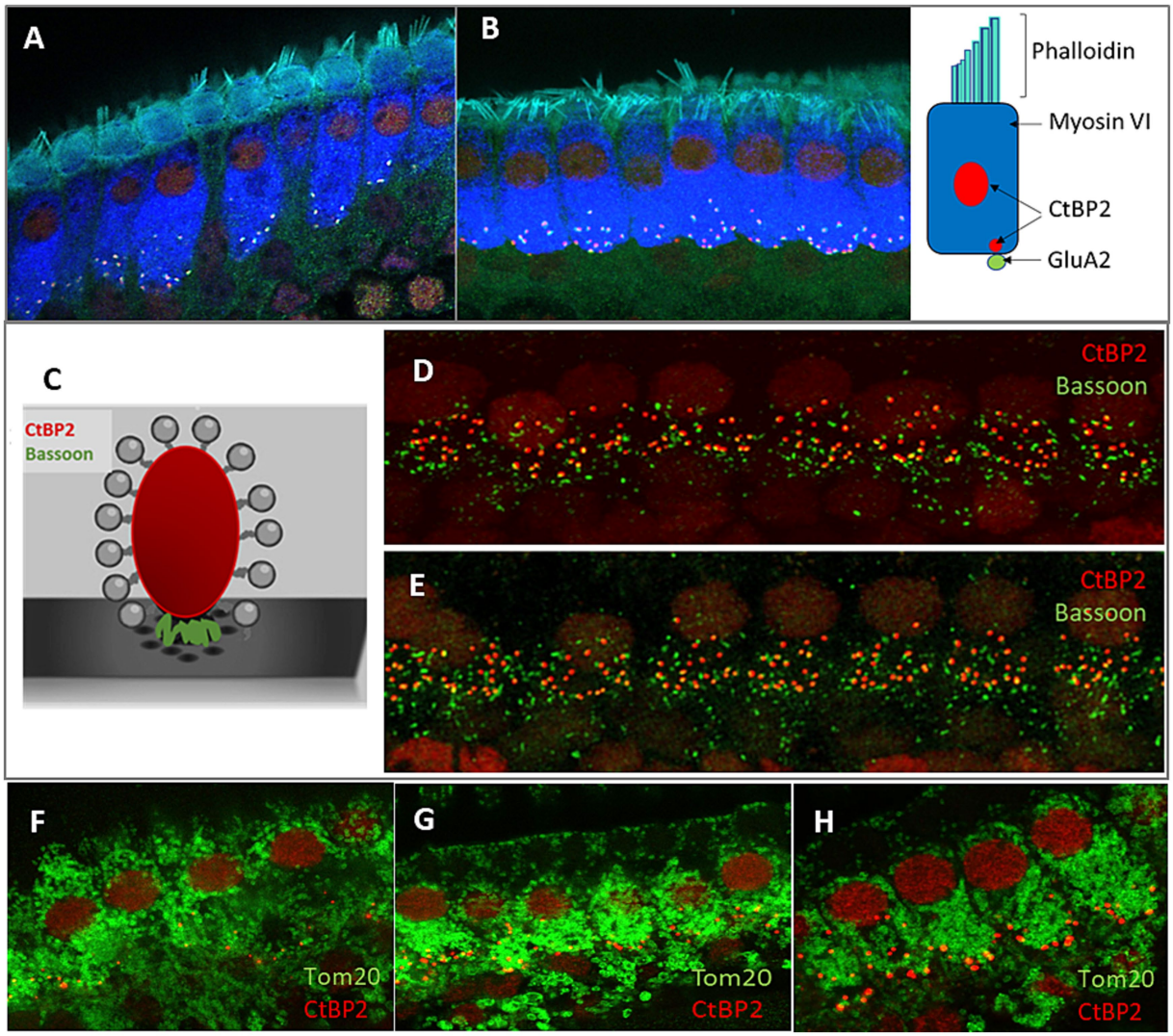

FIGURE 2
Analysis of the morphology of hair cells in P48 WT and *FMR1* KO mice. Representative images of inner hair cells (IHC) of the organ of Corti's from WT **(A)** and Fmr1FVB **(B)** mice. Schematic illustrations of ribbon synapse, a presynaptic markers, CtBP2 (red) and Bassoon (green), placed between ribeye and the presynaptic membrane **(C)**. Immunostaining with anti-CtBP2 antibody (red) and anti-Bassoon antibody (green) in WT **(D)** and Fmr1KO **(E)** mice. **(F–H)** Representative images of Tom20 as a marker for mitochondria in hair cells WT **(F)** and Fmr1KO **(G)** mice, immunostaining with anti-CtBP2 antibody (red) and anti-Tom20 (FL-145) antibody (green). Enlargement of inner hair cells in Fmr1KO mouse **(H)**, 63× objective.

block face scanning electron microscopy (SBF-SEM). The study was conducted at the developmental stage of P48.

First, we evaluated the overall morphology of the organ of Corti in *Fmr1* KO mice, and found no abnormalities in its organization. The sensory cells—inner hair cells (IHCs) and outer hair cells (OHCs)—were properly arranged along the basilar membrane, with the tectorial membrane positioned above them. Both IHCs and OHCs exhibited hair bundles, known as stereocilia (Figures 5A,B).

Next, we investigated the ultrastructure of *Fmr1* KO inner hair cells using transmission electron microscopy. Figure 5 presents representative images of IHCs from both *Fmr1* KO and wild-type (WT) cochleae. The overall morphology of *Fmr1* KO IHCs appeared comparable to that of WT cells, with well-defined stereocilia (Figures 5A,B). The shape of the Fmr1 KO IHCs, as well as the distribution of mitochondria and the nucleus, was similar to that observed in WT IHCs.

We observed typical postsynaptic densities and synaptic structures, including presynaptic dense bodies (ribbons) coated with synaptic vesicles. In some synapses, the ribbon was linked to the postsynaptic membrane via filamentous structures. Mitochondria were located beneath the cuticular plate and surrounding the nucleus, and were often associated with strands of intracellular membrane. The overall morphology of IHCs' mitochondria qualitatively appeared comparable to that of WT.

While transmission electron microscopy (TEM) provides high-resolution images of inner hair cells and ribbon synapses, it is limited in capturing the overall shape and morphology of entire cells. To address this question, we performed three-dimensional reconstructions of whole IHCs from both wild-type (WT) and *Fmr1*

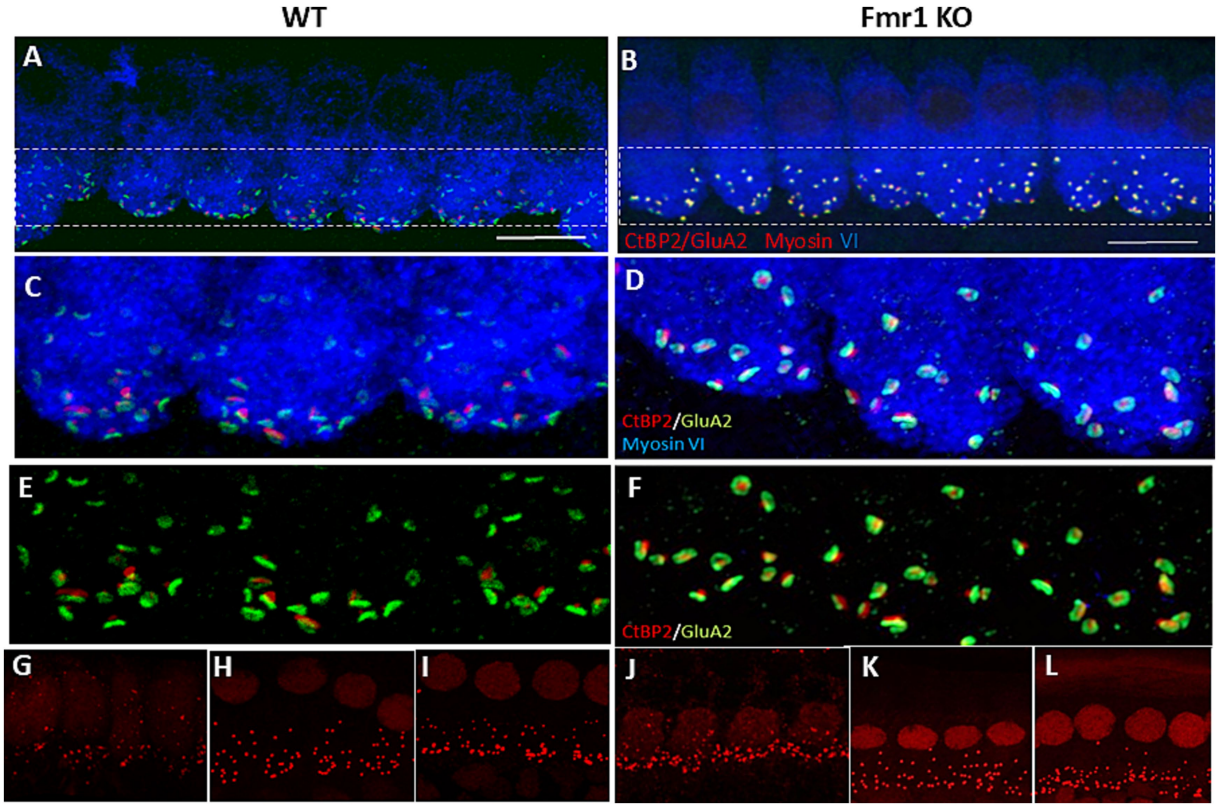

FIGURE 3
Immunofluorecent staining of IHCs and ribbon synapses in WT and *Fmr1*KO mice. **(A,B)** Representative images of the IHC of the organ of Corti's from P48 mice. White rectangular region is enlarged on **(C,D)** (63× objective). The basal part of the cell containing multiple synaptic contacts, a presynaptic marker, CtBP2 (red dots), a postsynaptic marker, GluA2 (green dots). **(E,F)** Enlargement of the synaptic layer of IHC, synapses are visible as red and green dots. **(G–L)** Visualization of synaptic ribbons at P5 **(G,J)**, P14 **(H,K)** and P48 **(I,L)** hair cells in WT and *Fmr1*KO mice with anti-CtBP2 antibody. The CtBP2 protein is present in ribbon synapses and cell nuclei. Scale bar 10 µm.

KO mice using serial block-face scanning electron microscopy (SBF-SEM).

Based on serial image reconstructions, we extracted specific morphological parameters, such as the mean IHC surface area, which showed no significant differences between the two genotypes (Figure 6D). We further reconstructed key cellular components, including the nucleus, mitochondria, synaptic ribbons, and nerve endings contacting individual IHCs. The mitochondrial distribution appeared uniform, and the localization of the nucleus was similar between *Fmr1* KO and WT mice.

Typically, inner hair cells exhibit a distinct flask-like shape, characterized by a constriction in the neck region. However, in the Fmr1KO mouse, the IHC displayed a more fusiform body shape compared to the wild-type control (Figure 6). The nucleus was positioned in the apical half of the cell, while mitochondria were primarily concentrated beneath the cuticular plate and surrounding the nucleus.

Afferent terminals were identified by the presence of a postsynaptic density on the afferent ending, accompanied by a corresponding synaptic ribbon (Figure 6, lower panel). We analyzed the spatial distribution of synaptic structures surrounding the IHCs and performed three-dimensional reconstructions of ribbon synapses. These reconstructions did not reveal any notable dysmorphologies in *Fmr1* KO mice compared to wild-type controls (Figure 6).

Quantitative analyses of both the number of ribbon synapses per cell (Figure 6E) and the number of afferent nerve endings contacting each IHC (Figure 6F) showed again no significant differences between WT and KO mice, indicating that the overall ultrastructure of IHCs in the inner ear remains intact in the absence of *FMRP*.

The quality of the SBF-SEM electron microscopy images was sufficiently good to enable detailed reconstruction of ribbon synapses for both mouse genotypes. For each genotype, we successfully reconstructed six synapses (Figure 7). We measured both the surface area of each synapse and the number of synaptic vesicles associated with it (Figures 7B,C). These analyses revealed no statistically significant differences between *Fmr1* KO and wild-type mice.

Discussion

This study provides new insights into the morphological and ultrastructural features of *Fmr1 KO* IHCs ribbon synapses, the first connection on the path that conveys the auditory information from the sensory cells to the brain. Analysis at early postnatal stages (P5, P14) showed delayed developmental maturation of IHC ribbon synapses in Fmr1 KO mice. Interestingly the ultrastructure of IHCs and their ribbons studied by electron microscopy in the adult mice have shown no specific dysmorphologies in Fmr1 KO mice. These findings suggest

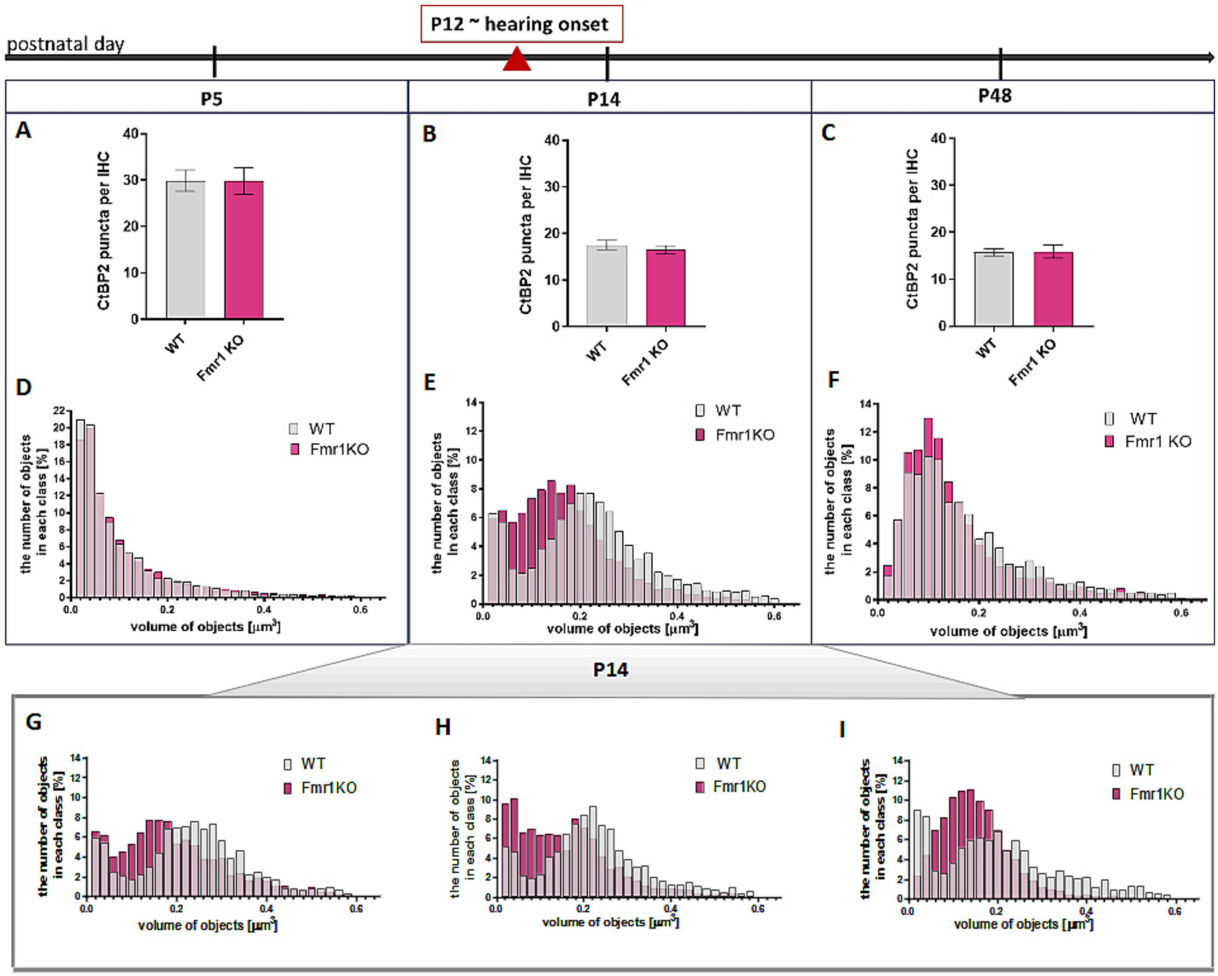

FIGURE 4
Changes in CtBP2/Ribeye in IHCs during development in apical turn of the cochlea Analysis of data based on anti-CtBP2 antibody staining against CtBP2/Ribeye protein (Figure 3). **(A–C)** Quantification of the number of CtBP2/Ribeye puncta per IHC at P5, P14, P48 WT and Fmr1KO mice. Data is presented as mean, error bars indicate SEM, (*t*-test; P5 *p*-value = 0.9812; P14 *p*-value = 0.4355, P48 *p*-value = 0.9225). **(D–F)** The histograms presenting the distribution of synapses according to their volume in apical turn of the cochlea of P5, P14, P48 mice. Y axis—number of objects in each size class (%), X axis—volume of objects (µm^3). Number of animals: P5: *N* = 3 WT *N* = 5 Fmr1 KO, P14: *N* = 6 WT, *N* = 8 Fmr1 KO, P48: *N* = 4 WT, *N* = 4 Fmr1 KO. Data is presented as a relative frequency distribution histogram; P5 *p*-value <0.0001; P14 *p*-value <0.0001; P48 *p*-value <0.0001; two sample Kolmogorov–Smirnov test. **(G–I)** The individual histograms for three independent litters of P14 mice (presented as combined data on panel **E**).

that delayed maturation of auditory hair cell synapses in the absence of FMRP may contribute to atypical auditory circuit development driven by early sensory experience.

Altered synaptic structure and function is a major hallmark of FXS neurons; however, these changes have been studied primarily in brain synapses (Bagni and Zukin, 2019). Patients with FXS have been shown to experience difficulties processing auditory information in the cortical regions of the brain. Neurodevelopmental disorders such as FXS characterize by the cell and circuit hyperexcitability (Goncalves et al., 2013; Zhang et al., 2014) often associated with such neurological symptoms as hypersensitivity, hyperarousal, hyperactivity, anxiety, and seizures (Penagarikano et al., 2007; Braat and Kooy, 2015). Additionally, *Fmr1* knockout (*Fmr1 KO*) mice exhibit increased sensitivity to sound. Electrophysiological studies on both *Fmr1 KO* mice and FXS patients suggest that the impairment may occur at an early stage of auditory information processing, potentially beginning at the level of spiral ganglion neurons (Rotschafer and Cramer, 2017; Arinami et al., 1988).

ABR studies on *Fmr1 KO* mice revealed altered responses compared to wild-type mice, with changes evident from the first wave peak, linked to spiral ganglion neuron activity (Rattay and Danner, 2014). The peak amplitude was reduced, and the sound threshold needed to evoke a response was elevated in *Fmr1 KO* mice (Rotschafer et al., 2015), indicating impaired hearing. In humans with FXS, increased N1 and P2 ERP amplitudes suggest heightened responses from auditory and associative cortices (Van der Molen et al., 2012a). Moreover, the N1 amplitude does not decrease with repeated tones, indicating reduced adaptation to auditory stimuli (Castren et al., 2003). ERP studies consistently report elevated N1 amplitudes and reduced habituation to repeated sounds in FXS (Rojas et al., 2001; Castren et al., 2003; Van der Molen et al., 2012a; Van der Molen et al., 2012b; Schneider et al., 2013; Dethridge et al., 2016). MEG studies also show enhanced auditory responses in FXS (Rojas et al., 2001).

This led us to investigate synaptic connections in the inner hair cells of *Fmr1 KO* mice. We started by confirming FMRP expression in IHCs of Corti. In the brain, FMRP is expressed at high levels in

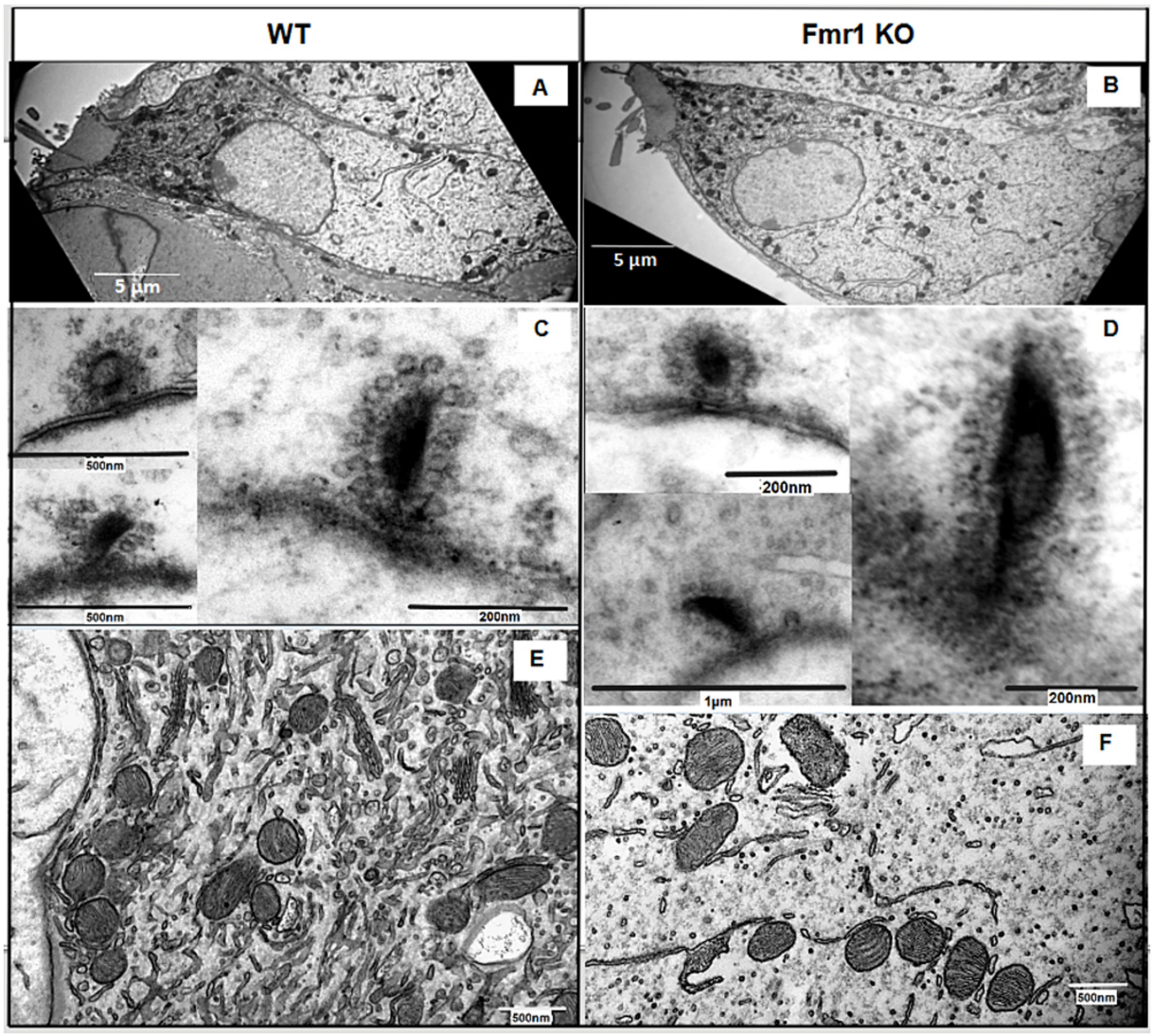

FIGURE 5
(A,B) Ultrastructural analysis of cochlear inner hair cells. Representative electron micrographs of the WT **(A)** and Fmr1KO inner hair cells **(B)** and their respective ribbon synapses surrounded by synaptic vehicles (synaptic vesicles are linked via filaments to the ribbon **C,D**) and mitochondria **(E,F)**.

auditory neurons at both cortical and subcortical levels (Beebe et al., 2014; Zorio et al., 2017; Yu et al., 2021). It was also shown to be present in hair cells and supporting cells of mice, rats, gerbils, and chickens, with a particularly high level in the immature hair cells during the prehearing period (Wang et al., 2023). We confirmed that FMRP is expressed in both inner and outer hair cells of WT mice, while *Fmr1 KO* mice lack this protein.

Since FMRP plays a critical role in synaptic development and plasticity, its absence may contribute to synaptic alterations in *Fmr1 KO* IHCs. We measured the number and volume of ribbon synapses in the IHCs of *Fmr1 KO* mice at the age of P5, P14 and P48. Before the onset of hearing, ribbon synapses in inner hair cells undergo significant molecular assembly and structural and functional maturation. During this process, synaptic contacts shift from multiple small active zones (AZs) to a single, larger one. This maturation involves the fusion of ribbon precursors with membrane-anchored ribbons, which can also merge with each other. These fusion events are most commonly observed around postnatal day 12 (P12), aligning with the onset of hearing in mice (Michanski et al., 2019).

We found that the average size of synaptic ribbons was significantly smaller in *Fmr1 KO* mice at P14 and remained slightly reduced in adulthood. That may reflect delayed maturation of ribbon synapses in the IHCs of *Fmr1 KO* mice. The total number of synapses per IHC was comparable between genotypes, but decreased with age as expected (Michanski et al., 2019). This suggests that FMRP is involved in the postnatal maturation of ribbon synapses, and its lack in Fmar1 KO mice is potentially affecting synaptic function and auditory processing. A higher proportion of smaller ribbons in *Fmr1 KO* mice indicates an alteration in synaptic developmental maturation, as ribbon size is linked to synaptic activity and neurotransmitter release efficiency (Mehta et al., 2013). The presence of GluA2-positive AMPA receptors at the postsynaptic side suggests that glutamatergic transmission is preserved; however, the observed differences in ribbon size in the critical age of development may contribute to abnormal development of circuits induced by auditory experience.

10.3389/fnmol.2025.1604262

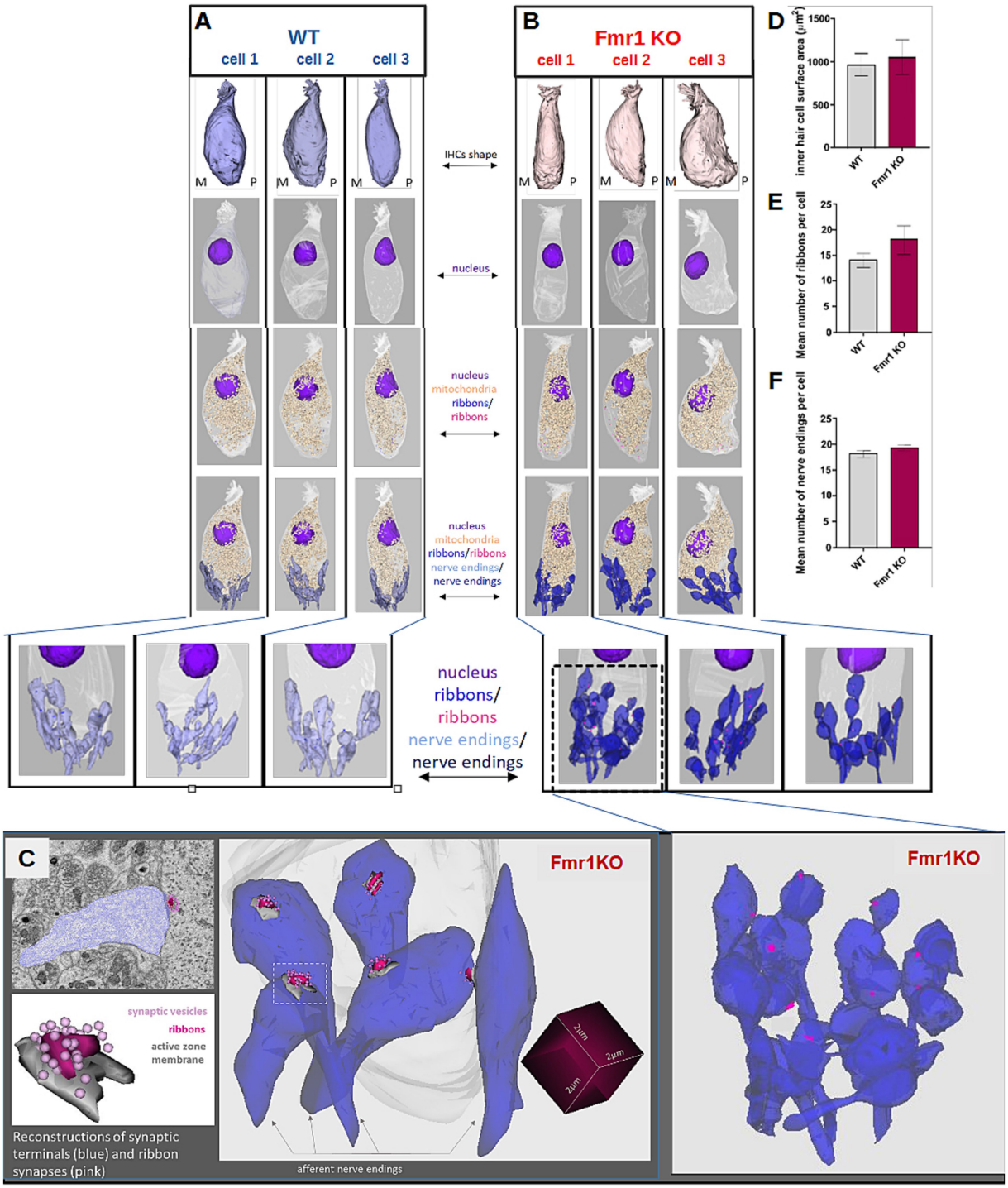

FIGURE 6
Detailed ultrastructural analysis of inner hair cells from adult (P48) WT (**A**, left pannel) and *Fmr1* KO mice (**B**, right panel). Three-dimensional reconstructions of IHCs shape, nucleus, mitochondria, ribbons, and nerve endings were obtained by serial image reconstruction from SBF-SEM. **(C)** Enlargement of the reconstructed nerve endings, ribbons, active zone membranes and synaptic vesicles **(D)** inner hair cell surface area WT vs. *Fmr1KO*, **(E)** mean number of ribbons per cell WT vs. *Fmr1KO*, **(F)** mean number of nerve endings per cell WT vs. *Fmr1KO*. Data is presented as mean, error bars indicate SEM, Mann–Whitney nonparametric test p-value >0.05.

The overall morphology of IHCs did not differ between the genotypes. The localization of Bassoon, a key presynaptic scaffolding protein, overlapped with synaptic ribbons in both WT and *Fmr1 KO* mice, suggesting that FMRP deletion does not affect the anchoring of ribbons to the presynaptic membrane. However, distinct Bassoon-positive signals that did not co-localize with CtBP2-positive ribbons were detected, likely originating from efferent nerve terminals. This raises the possibility that alterations in efferent synaptic input may accompany the observed changes in ribbon synapse maturation.

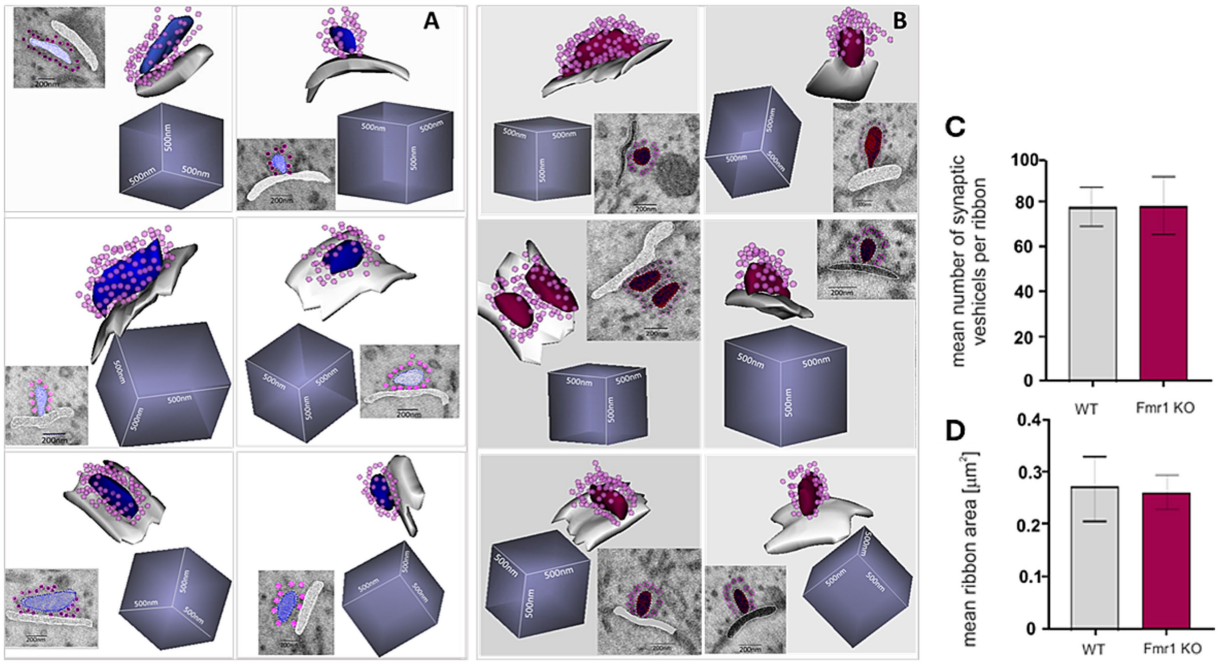

FIGURE 7
Ultrastructure of reconstructed ribbon synapses from WT **(A)** and Fmr1KO **(B)** organ of Corti revealed by SBF-SEM. Mean number of synaptic vesicles per ribbon **(C)** and mean ribbon area **(D)** (n = 6 synapses/genotype). The length of the side of the cube in each reconstruction is 500 nm.

Ultrastructural analyses using transmission electron microscopy (TEM) and serial block-face scanning electron microscopy (SBF-SEM) further revealed that the overall morphology of IHCs and the organ of Corti remained intact in *Fmr1 KO* mice. The spatial organization of stereocilia, mitochondria, and nuclei appeared similar between WT and *Fmr1 KO* IHCs, indicating that gross cellular morphology is preserved despite the absence of FMRP.

In our previous study we detected abnormalities in the morphology of the mitochondria in *Fmr1 KO* brain (Kuzniewska et al., 2019). Apparently in the IHCs of *Fmr1 KO* mice organ of Corti the mitochondria displayed perfectly normal shape and size and looked very similar to WT.

Three-dimensional reconstructions of ribbon synapses provided additional confirmation that the synaptic architecture of IHCs in *Fmr1 KO* mice remains largely unaltered. Synaptic ribbons were positioned opposite postsynaptic densities, and no major dysmorphologies were observed. Nevertheless, given the differences in ribbon size distribution, it is possible that synaptic function is subtly impaired, potentially contributing to auditory deficits commonly associated with fragile X syndrome.

Taken together, our findings indicate that *Fmr1 KO* mice exhibit a delay in ribbon synapse maturation without major structural abnormalities in IHCs. This suggests that FMRP is not essential for the initial formation of ribbon synapses but may play a crucial role in their postnatal development and refinement. Future studies should focus on functional assessments, such as electrophysiological recordings, to determine whether the observed morphological changes translate into synaptic transmission deficits. Understanding the impact of FMRP loss on auditory processing at a cellular level could provide valuable insights into the auditory impairments seen in fragile X syndrome and related neurodevelopmental disorders.

Data availability statement

The raw data supporting the conclusions of this article will be made available by the authors, without undue reservation.

Ethics statement

The animal study was approved by First Local Ethical Commission for Animal Experiments in Warsaw. The study was conducted in accordance with the local legislation and institutional requirements.

Author contributions

MC: Conceptualization, Writing – original draft, Writing – review & editing, Data curation, Investigation, Methodology, Validation, Visualization. AS-J: Data curation, Investigation, Writing – original draft, Writing – review & editing. MD: Writing – original draft, Writing – review & editing, Conceptualization, Formal analysis, Funding acquisition, Project administration, Resources, Supervision.

Funding

The author(s) declare that financial support was received for the research and/or publication of this article. This work was supported by the National Science Centre, Poland, under the OPUS Programme Grant 2017/27/B/NZ4/01169 for MD.

Acknowledgments

Electron microscopy experiments were performed at the Laboratory of Imaging Tissue Structure and Function which serves as an imaging core facility at the Nencki Institute of Experimental Biology in Warsaw and is part of the infrastructure of the Polish Euro-BioImaging Node financed by Polish Ministry of Science and Higher Education Contract No. 2022/WK/05; Polish Euro-BioImaging Node "Advanced Light Microscopy Node". We would like to thank Dr Piotr Kazmierczak and Dr Maciej Winiarski for methodological support in this project.

Conflict of interest

The authors declare that the research was conducted in the absence of any commercial or financial relationships that could be construed as a potential conflict of interest.

Generative AI statement

The authors declare that no Gen AI was used in the creation of this manuscript.

Any alternative text (alt text) provided alongside figures in this article has been generated by Frontiers with the support of artificial intelligence and reasonable efforts have been made to ensure accuracy, including review by the authors wherever possible. If you identify any issues, please contact us.

Publisher's note

References

Arinami, T., Sato, M., Nakajima, S., and Kondo, I. (1988). Auditory brain-stem responses in the fragile X syndrome. *Am. J. Hum. Genet.* 43, 46–51

Bagni, C., and Zukin, R. S. (2019). A synaptic perspective of fragile X syndrome and autism spectrum disorders. *Neuron* 101, 1070–1088. doi: 10.1016/j.neuron.2019.02.041

Beebe, K., Wang, Y., and Kulesza, R. (2014). Distribution of fragile X mental retardation protein in the human auditory brainstem. *Neuroscience* 273, 79–91. doi: 10.1016/j.neuroscience.2014.05.006

Braat, S., and Kooy, R. F. (2015). The Gabaa receptor as a therapeutic target for neurodevelopmental disorders. *Neuron* 86, 1119–1130. doi: 10.1016/j.neuron.2015.03.042

Bullen, A., West, T., Moores, C., Ashmore, J., Fleck, R. A., Maclellan-Gibson, K., et al. (2015). Association of intracellular and synaptic organization in cochlear inner hair cells revealed by 3D electron microscopy. *J. Cell Sci.* 128, 2529–2540. doi: 10.1242/jcs.170761

Castren, M., Paakkonen, A., Tarkka, I. M., Ryynanen, M., and Partanen, J. (2003). Augmentation of auditory N1 in children with fragile X syndrome. *Brain Topogr.* 15, 165–171. doi: 10.1023/A:1022606200636

Comery, T. A., Harris, J. B., Willems, P. J., Oostra, B. A., Irwin, S. A., Weiler, I. J., et al. (1997). Abnormal dendritic spines in fragile X knockout mice: maturation and pruning deficits. *Proc. Natl. Acad. Sci. U.S.A.* 94, 5401–5404. doi: 10.1073/pnas.94.10.5401

Crawford, D. C., Acuna, J. M., and Sherman, S. L. (2001). Fmr1 and the fragile X syndrome: human genome epidemiology review. *Genet. Med.* 3, 359–371. doi: 10.1097/00125817-200109000-00006

Deerinck, T. J., Bushong, E. A., Lev-Ram, V., Shu, X., Tsien, R. Y., and Ellisman, M. H. (2010). Enhancing serial block-face scanning Electron microscopy to enable high resolution 3-D nanohistology of cells and tissues. *Microsc. Microanal.* 16, 1138–1139. doi: 10.1017/S1431927610055170

Dethridge, L. E., White, S. P., Mosconi, M. W., Wang, J., Byerly, M. J., and Sweeney, J. A. (2016). Reduced habituation of auditory evoked potentials indicate cortical hyper-excitability in fragile X syndrome. *Transl. Psychiatry* 6:e787. doi: 10.1038/tp.2016.48

Fiala, J. C. (2005). Reconstruct: a free editor for serial section microscopy. *J. Microsc.* 218, 52–61. doi: 10.1111/j.1365-2818.2005.01466.x

Glowatzki, E., and Fuchs, P. A. (2002). Transmitter release at the hair cell ribbon synapse. *Nat. Neurosci.* 5, 147–154. doi: 10.1038/nn796

Goncalves, J. T., Anstey, J. E., Golshani, P., and Portera-Cailliau, C. (2013). Circuit level defects in the developing neocortex of fragile X mice. *Nat. Neurosci.* 16, 903–909. doi: 10.1038/nn.3415

Hagerman, R. J., Berry-Kravis, E., Hazlett, H. C., Bailey, D. B. Jr., Moine, H., Kooy, R. F., et al. (2017). Fragile X syndrome. *Nat. Rev. Dis. Primers* 3:17065. doi: 10.1038/nrdp.2017.65

Hagerman, R. J., Ono, M. Y., and Hagerman, P. J. (2005). Recent advances in fragile X: a model for autism and neurodegeneration. *Curr. Opin. Psychiatry* 18, 490–496. doi: 10.1097/01.yco.0000179485.39520.b0

Kuzniewska, B. C. D., Wasilewski, M., Sakowska, P., Milek, J., Kulinski, T. M., Kozielewicz, P., et al. (2019). Mitochondria biogenesis in the synapse is supported by local translation. *EMBO Rep*. 21. doi: 10.15252/embr.201948882

Liberman, M. C., and Kujawa, S. G. (2017). Cochlear synaptopathy in acquired sensorineural hearing loss: manifestations and mechanisms. *Hear. Res.* 349, 138–147. doi: 10.1016/j.heares.2017.01.003

Mehta, B., Snellman, J., Chen, S., Li, W., and Zenisek, D. (2013). Synaptic ribbons influence the size and frequency of miniature-like evoked postsynaptic currents. *Neuron* 77, 516–527. doi: 10.1016/j.neuron.2012.11.024

Michanski, S., Smaluch, K., Steyer, A. M., Chakrabarti, R., Setz, C., Oestreicher, D., et al. (2019). Mapping developmental maturation of inner hair cell ribbon synapses in the apical mouse cochlea. *Proc. Natl. Acad. Sci. U.S.A.* 116, 6415–6424. doi: 10.1073/pnas.1812029116

Penagarikano, O., Mulle, J. G., and Warren, S. T. (2007). The pathophysiology of fragile X syndrome. *Annu. Rev. Genomics Hum. Genet.* 8, 109–129. doi: 10.1146/annurev.genom.8.080706.092249

Rais, M., Binder, D. K., Razak, K. A., and Ethell, I. M. (2018). Sensory processing phenotypes in fragile X syndrome. *ASN Neuro* 10:1759091418801092. doi: 10.1177/1759091418801092

Rattay, F., and Danner, S. M. (2014). Peak I of the human auditory brainstem response results from the somatic regions of type I spiral ganglion cells: evidence from computer modeling. *Hear. Res.* 315, 67–79. doi: 10.1016/j.heares.2014.07.001

Razak, K. A., Binder, D. K., and Ethell, I. M. (2021). Neural correlates of auditory hypersensitivity in fragile X syndrome. *Front Psychiatry* 12:720752. doi: 10.3389/fpsyt.2021.720752

Rojas, D. C., Benkers, T. L., Rogers, S. J., Teale, P. D., Reite, M. L., and Hagerman, R. J. (2001). Auditory evoked magnetic fields in adults with fragile X syndrome. *Neuroreport* 12, 2573–2576. doi: 10.1097/00001756-200108080-00056

Rotschafer, S. E., and Cramer, K. S. (2017). Developmental emergence of phenotypes in the auditory brainstem nuclei of Fmr1 knockout mice. *eNeuro* 4:ENEURO.0264-17.2017. doi: 10.1523/ENEURO.0264-17.2017

Rotschafer, S. E., Marshak, S., and Cramer, K. S. (2015). Deletion of Fmr1 alters function and synaptic inputs in the auditory brainstem. *PLoS One* 10:e0117266. doi: 10.1371/journal.pone.0117266

Rotschafer, S., and Razak, K. (2013). Altered auditory processing in a mouse model of fragile X syndrome. *Brain Res.* 1506, 12–24. doi: 10.1016/j.brainres.2013.02.038

Rotschafer, S. E., and Razak, K. A. (2014). Auditory processing in fragile X syndrome. *Front. Cell. Neurosci.* 8:19. doi: 10.3389/fncel.2014.00019

Schneider, A., Leigh, M. J., Adams, P., Nanakul, R., Chechi, T., Olichney, J., et al. (2013). Electrocortical changes associated with minocycline treatment in fragile X syndrome. *J. Psychopharmacol.* 27, 956–963. doi: 10.1177/0269881113494105

Sinclair, D., Oranje, B., Razak, K. A., Siegel, S. J., and Schmid, S. (2017). Sensory processing in autism spectrum disorders and fragile X syndrome-from the clinic to animal models. *Neurosci. Biobehav. Rev.* 76, 235–253. doi: 10.1016/j.neubiorev.2016.05.029

Van der Molen, M. J., Van der Molen, M. W., Ridderinkhof, K. R., Hamel, B. C., Curfs, L. M., and Ramakers, G. J. (2012a). Auditory and visual cortical activity during selective attention in fragile X syndrome: a cascade of processing deficiencies. *Clin. Neurophysiol.* 123, 720–729. doi: 10.1016/j.clinph.2011.08.023

Van der Molen, M. J., Van der Molen, M. W., Ridderinkhof, K. R., Hamel, B. C., Curfs, L. M., and Ramakers, G. J. (2012b). Auditory change detection in fragile X syndrome males: a brain potential study. *Clin. Neurophysiol.* 123, 1309–1318. doi: 10.1016/j.clinph.2011.11.039

Wang, X., Fan, Q., Yu, X., and Wang, Y. (2023). Cellular distribution of the fragile X mental retardation protein in the inner ear: a developmental and comparative study in the mouse, rat, gerbil, and chicken. *J. Comp. Neurol.* 531, 149–169. doi: 10.1002/cne.25420

Wichmann, C., and Moser, T. (2015). Relating structure and function of inner hair cell ribbon synapses. *Cell Tissue Res.* 361, 95–114. doi: 10.1007/s00441-014-2102-7

Yu, X., Wang, X., Sakano, H., Zorio, D. A. R., and Wang, Y. (2021). Dynamics of the fragile X mental retardation protein correlates with cellular and synaptic properties in primary auditory neurons following afferent deprivation. *J. Comp. Neurol.* 529, 481–500. doi: 10.1002/cne.24959

Zhang, Y., Bonnan, A., Bony, G., Ferezou, I., Pietropaolo, S., Ginger, M., et al. (2014). Dendritic channelopathies contribute to neocortical and sensory hyperexcitability in *Fmr1*$^{-/y}$ mice. *Nat. Neurosci.* 17, 1701–1709. doi: 10.1038/nn.3864

Zorio, D. A., Jackson, C. M., Liu, Y., Rubel, E. W., and Wang, Y. (2017). Cellular distribution of the fragile X mental retardation protein in the mouse brain. *J. Comp. Neurol.* 525, 818–849. doi: 10.1002/cne.24100